Outer-Shell and Inner-Shell Coordination of Phosphate Group to Hydrated Metal Ions (Mg^{2+}, Cu^{2+}, Zn^{2+}, Cd^{2+}) in the Presence and Absence of Nucleobase. The Role of Nonelectrostatic Effects

Lubomír Rulíšek[†,§] and Jiří Šponer*[,‡,§,#]

Institute of Biophysics, Academy of Sciences of the Czech Republic, Královopolská 135, 612 65 Brno, Czech Republic, J. Heyrovský Institute of Physical Chemistry, Academy of Sciences of the Czech Republic and Center for Complex Molecular Systems and Biomolecules, Dolejškova 3, 182 23 Prague, Czech Republic, and Institute of Organic Chemistry and Biochemistry, Academy of Sciences of the Czech Republic, Flemigovo náměstí. 2, 166 10 Prague 6, Czech Republic

Received: September 24, 2002; In Final Form: December 5, 2002

Inner-shell binding of selected hydrated metal ions (Mg^{2+}, Cu^{2+}, Zn^{2+}, and Cd^{2+}) to the guanine N7 position accompanied with outer- and inner-shell binding to an anionic phosphate group is investigated using quantum chemical approaches. The study is focused on the mutual interplay between the metal−phosphate and metal-nucleobase binding and the role of nonelectrostatic effects in the metal binding as these contributions are not included in conventional empirical force fields. The analysis of the equilibrium structures and the energy decompositions reveal that these effects substantially contribute to the differences in the coordination behavior of the studied metal ions. The Zn^{2+} and Cd^{2+} cations show a clear preference to bind to N7 of guanine compared to Mg^{2+}. The selectivity is of ca. 3−4 kcal·mol^{-1} on the energy scale. This energy difference is sufficient to provide enough binding selectivity in the condensed phase where the dominant pair electrostatic terms (ion−ion, molecule−ion) are attenuated. Cu^{2+} shows even stronger relative preference for N7 binding and it has also different coordination requirements. The nucleobase N7 metal binding causes ca. 20−30 kcal·mol^{-1} destabilization of the metal−phosphate outer-shell binding, entirely due to nonelectrostatic effects. The calculations were done with the Becke3LYP DFT method and extended basis set of atomic orbitals for energy evaluations. This technique provides a very accurate description of metal cation containing clusters. It is demonstrated for Mg^{2+} systems using reference RI-MP2/TZVPP calculations showing excellent agreement with the DFT approach regarding both molecular structures and energies. Most systems were also optimized with the HF/6-31G* method supplemented by MP2 single point energy evaluations. The later method was utilized in many recent studies of cation binding to nucleic acids and is shown here to provide meaningful results. Validity of the conclusions based on calculations utilizing the gas-phase cluster model is further verified by additional calculations of the solvation effects. The present study reveals important qualitative aspects of selective metal binding to nucleic acids, provides useful comparison of different computational methods, and furnishes reference data for verification and parametrization of other computational methods including force fields.

I. Introduction

Metal ions are widely present in biological systems and have an indispensable role in the structure and function in many of the fundamental blocks of living organisms. Hence, plenty of experimental and theoretical studies have been carried out to elucidate the mechanisms of metalloenzyme action (including transition state structures, proton and electron transfer),[1] structural aspects of metal-binding sites in DNA/RNA/proteins,[2−6] and the energetics of biocatalysis.[7] The recent advances in the field are documented in several reviews.[4j,8,9]

One of the most important properties of biomolecular systems is the relationship between molecular structures and energies. Molecular structures can be efficiently studied by atomic-resolution experimental techniques,[4] but it is considerably more difficult to complement the structural data by unambiguous information about the energies. A promising way to unravel the fundamental links between structures and energies in bioinorganic systems is an application of modern computational methods. Because the interactions of metal cations are associated with substantial charge-transfer effects, the usage of methods based on the approximate pair additivity of the many-body interactions (e.g., common empirical force fields) is sharply limited. These systems should be preferably studied using correlated quantum-chemical methods.

Besides yielding crude structural and energetical characterization of the studied systems, a careful interpretation of the theoretical data and their comparisons with the experimental ones yields insights into more general concepts, such as the reaction pathway and specificity of the metal ion binding in biomolecules.[10] It is the latter phenomenon that opens the central question of bioinorganic chemistry: "Why has the particular metal ion been selected for performing certain biological tasks?"

* Corresponding author. E-mail: sponer@ibp.cz. Fax: (420 5) 4121 2179.
† Institute of Organic Chemistry and Biochemistry.
§ Center for Complex Molecular Systems and Biomolecules.
‡ J. Heyrovský Institute of Physical Chemistry.
# Institute of Biophysics.

10.1021/jp027058f CCC: $25.00
Published on Web 01/24/2003

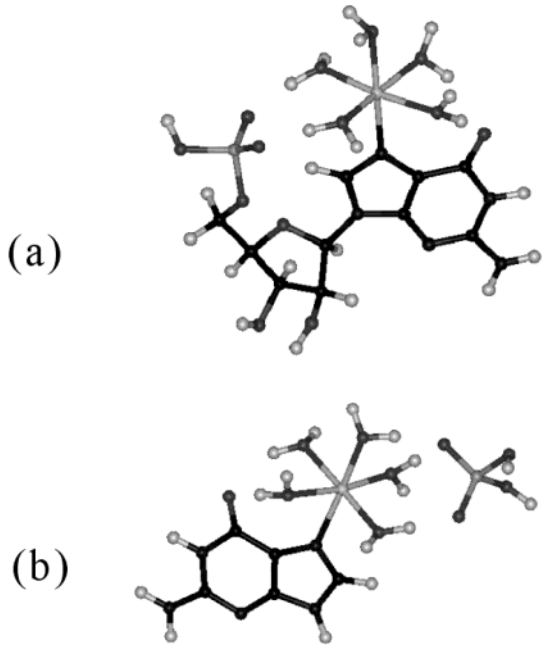

Figure 1. (a) Complete nucleotide $dGMP^{-1}$ interacting with a hydrated metal cation M_H.[2b] (b) After deleting the sugar unit, the system has been separated into three particles: nucleobase, phosphate group, and the hydrated metal cation.

It is often assumed that the major determinants of the metal cations selectivity are their size and charge. However, the selectivity of cations is also substantially affected by contributions originating in their molecular orbital architecture. Note that, for example, Zn^{2+} and Mg^{2+} cations have basically the same radius whereas their interactions often differ.

Recent efforts to evaluate the specificity of metal ion binding in the metalloproteins[11−14] have shown that on the basis of relative values of computed quantum chemical properties (differences in the series of metal ions), it is possible to make quantitative extensions of the basic theories of coordination chemistry. These include the HSAB (hard and soft acids and bases) principle of Parr and Pearson[15] and the Irving−Williams (IW) series of stability constants.[16] However, it must be noticed that very accurate computational schemes (guaranteeing the accuracy of 1−2 kcal·mol^{-1}, at least in the relative values) should be used.[17] It is because an uncertainty of 1.3 kcal·mol^{-1} in the value of ΔE_{int}, as the approximation of ΔG^0 for a given process, leads to an error of 1 in log K (e.g., stability constants). It is a very small difference from the computational point of view, but it becomes relevant for practical considerations dealing with metal ion specificity.

In the past few years, systematic QM studies were carried out to characterize various aspects of metal cation binding to nucleic acid constituents, mainly to nucleobases.[2,18−25] The calculations addressed the selectivity of a metal cation binding to the purine N7 position,[2] the effects of metalation of nucleobases on the strength of base pairing,[2,18] and various proton shift processes such as tautomerism, protonation, deprotonation, and proton transfer.[2b,22] Additional studies then focused on the interactions between metal cations and the phosphate group.[2b,25]

Recently, we have characterized direct (inner-shell) N7 binding of selected hydrated cations to nucleotides, revealing the key role of screening effects exerted by the negatively charged sugar−phosphate segment (Figure 1a).[2b] As this study raised many questions regarding the energetic balance between the different contributions to the overall interaction energy (e.g., three-body energetical terms) or possible variations in the [metal ion−nucleobase−phosphate] binding modes, we attempt to analyze these aspects in the present study. To achieve this goal, the sugar unit linking the nucleobase with a negatively charged phosphate group has been deleted (Figure 1b) and the nucleotide monomer split into two subsystems: the nucleobase and the phosphate group.

It allows separate evaluation of metal−nucleobase and metal−phosphate contributions together with the nonadditivity of interactions. Such decomposition is not possible with the complete nucleotide structure. The calculations are aimed to reveal how the metal−base and metal−phosphate interactions electronically influence each other (cooperativity of interactions). We also investigate whether the nucleobase binding may affect the hydrogen-bonding ability of the first hydration shell of the cation toward the phosphate group. The calculations provide insights into the origins and magnitude of the different balance of inner-shell cation binding to the guanine N7 position with respect to inner- and outer-shell binding to the phosphate group and hydration of the ion. All these contributions predetermine the biochemical roles of the cations. For obvious reasons, we could analyze only a limited number of coordination arrangements. Nevertheless, we assume that the four binding motifs studied here are quite representative, as they are closely related to the reference states of these metal ions (octahedral hexaaqua complexes) and all four studied binding patterns have been already documented in atomic-resolution oligonucleotide X-ray studies.[4,25a] The calculations provide not only the qualitative analysis of interactions but also useful reference data for verification and parametrization of a new class of polarizable force fields that we consider as the only type of empirical approach applicable to studies of transition metal centers.[12b,c,21]

Electrostatic and Nonelectrostatic Effects. The metal cation binding is associated with substantial polarization and charge-transfer contributions that cannot be described by a simple pair additive electrostatic term or empirical potential. These contributions are often quoted as *nonelectrostatic effects* in the literature, although, strictly speaking, polarization originates in Coulombic terms of the Hamiltonian. This is to distinguish them from *pair-additive long-range electrostatic effect*s well described by empirical potential with constant point charges. Note that the vast majority of computational studies of biomolecular systems are carried out using simple force fields neglecting polarization and charge transfer. It is also well established that the long-range electrostatic effects, especially in ionic systems, are counterbalanced by polar solvents relevant for biomolecular systems.[22] All the nonelectrostatic effects (as defined above) are considerably less affected by the environment and remain expressed in bioinorganic experiments.[22] That is another reason to separate long-range electrostatic and nonelectrostatic effects, as suggested above.

Studied Systems. Four metal ions are studied in this work, namely, Mg^{2+}, Zn^{2+}, Cd^{2+}, and Cu^{2+}. All four belong to the most abundant metal ions in biological material. On the other hand, they are quite distinctive from the coordination chemistry point of view and represent thus a wide sample of species to study the various contributions determining the selectivity in metal cation−DNA interactions, especially those not merely related to the size of the cation. Magnesium(II) and zinc(II) are the most relevant ions for the structure and function of RNA/DNA, whereas cadmium(II), a representative of soft metal ions, can be considered as a xenobiotic ion. The copper(II) is a d^9 open shell cation and has not been considered in preceding theoretical studies on DNA−metal cation interactions. Though

it is an abundant metal ion in the structures of metalloproteins, it is included here mainly from its being at the top of IW series of stability constants (i.e., having the highest *average* binding strength).

With each ion, two model systems have been studied. The first one is the [guanine−$M(H_2O)_5$−(H_2PO_4)]$^+$ complex, where M denotes a divalent metal cation. In the following, this system is abbreviated as G−M_H−P. The initial geometry was taken from the previously published structure of GMP^{-1} (guanosine monophosphate) interacting with the pentahydrated Mg^{2+} ion (cf. Figure 1 and Supporting Information).[2b] The sugar unit has been deleted and subsystems (nucleobase and phosphate) capped with hydrogens at both ends. The metal cation is directly bound to the guanine N7 position (inner-shell binding), whereas the interaction between the metal cation and the phosphate group is water-mediated (outer-shell binding). In the second system, the guanine base has been replaced by a water molecule and this is denoted as [(H_2O)−$M(H_2O)_5$−(H_2PO_4)]$^+$, and abbreviated as W−M_H−P. The notation indicates that in the interaction energy calculations (see below), one water molecule (replacing the base) is formally treated as a separate subsystem and the $M_H = [M(H_2O)_5]^{2+}$ complex represents another subsystem. Thus, the whole cluster is separated into three subunits. Note, however, that structure optimizations were carried out by imposing no constraint and all intramolecular and intermolecular parameters were optimized.

We have also investigated an alternative geometry for both systems, where one water molecule is expelled into the second hydration shell with a simultaneous formation of an inner-shell complex between M and P. We designate these systems as G−M_H−P_{in} and W−M_H−P_{in}. This geometry has been originally obtained when attempting to optimize the W−Cd_H−P system at the Hartree−Fock level. We do not claim that the X−M_H−P_{in} is the global minimum for inner-shell binding to P; nevertheless, it should be a representative model for such structures.

Geometrical constraints have been imposed on complexes of Cu^{2+} ion, because it is Jahn−Teller unstable in octahedral coordination geometry and the X−Cu_H−P systems convert into a five-coordinated arrangement with one water molecule and the phosphate in the outer-shell (substantially different from both X−M_H−P and X−M_H−P_{in} geometries) in the course of molecular geometry optimization. The constraints were freezing L−M−L bond angles at the values corresponding to octahedral geometry (i.e., 90° for ligands in cis and 180° for ligands in trans mutual orientation). This approach enables the comparison of the decompositions of interaction energies between studied TM ions.

II. Computational Details

Most calculations were performed with the Gaussian 98 program suite.[26]

For density functional theory (DFT) calculations, the three-parameter functional developed by Becke,[27] which combines the Becke's gradient-corrected exchange functional and the Lee−Yang−Parr and Vosko-Wilk-Nusair correlation functionals[28] with part of the exact Hartree−Fock exchange energy, has been employed (denoted as B3LYP).

The DFT optimizations of molecular geometries were carried out using the 6-31G basis set augmented by diffuse functions (s,2p,d) set for transition metals (TMs), sp functions for other heavy elements, and a single set of polarization functions: f for TMs, and d for other heavy elements. Single point energy calculations on the optimized geometries were carried out with a considerably improved basis set using the triple-ζ (TZ) basis set of Watchers and Hay[29] for the first row transition metals (Cu and Zn), and standard 6-311G for other elements (H, C, N, O, P)[30] augmented by the same diffuse functions as above with further addition of s functions for hydrogens and the following sets of polarization functions: 2fg for TMs, 2df for other heavy atoms, 2pd for hydrogens. The exponents of all diffuse and polarization functions were used as implemented in Gaussian 98 and the described basis sets have been specified via 6-31+G-(d), and 6-311++G(2df,2pd) keywords.

For Cd^{2+} effective core potential (ECP) of Stevens and coworkers[31] has been used (denoted SBKJ). To achieve consistency with the above-described basis sets used for the first row TMs, the original valence basis set was further augmented with the following uncontracted GTO basis functions: diffuse d functions (α_d(Cd) = 0.075) and f (α_f(Cd) = 0.775) and 2fg (α_{1f} (Cd) = 2.0, α_{2f} (Cd) = 0.3, α_g (Cd) = 0.775) sets of polarization functions, corresponding to 6-31+G(d) and 6-311++G(2df,2pd) basis sets, respectively.

The above DFT/B3LYP scheme has been shown to yield accurate complexation (interaction) energies of metal ions in the model metal-binding sites[17] and is therefore expected to describe the studied systems with a reasonable accuracy.

To estimate the convergence and method-dependence of the results, we have also carried out optimizations at the Hartree−Fock (HF) level supplemented by single point evaluation of the interaction energies using the second-order Moeller−Plesset method (MP2). These calculations were done using smaller 6-31G(d) basis set except of Zn^{2+} and Cd^{2+} which were described by the Christiansen's ECP.[32]

In addition, reference calculations were carried out for Mg^{2+} structures using the RI-MP2 (Resolution of the Identity MP2) method with an extended TZVPP basis set of atomic orbitals using the Turbomole code.[33] The RI-MP2 method is very efficient and provides results close to identical to those from the MP2 procedure for base pairing and stacking.[34] The RI-MP2/TZVPP method actually provides results identical to those obtained with the MP2/cc-pVTZ method with only a fraction of computer requirements.[34]

The solvation Gibbs energies, ΔG_{solv}, have been estimated using the COSMO method as implemented in Gaussian 98 (CPCM).[35] The standard dielectric constant for water has been used ($\epsilon_r = 78.39$).

Definition of Interaction Energy. The interaction energy of a trimer, ΔE_{ABC}, can be expressed in two ways, (i) as a difference of the electronic energy of the complex and the monomers:[2]

$$\Delta E_{ABC} = E_{ABC} - (E_A + E_B + E_C) \quad (1)$$

or (ii) as a sum of three pairwise dimer interaction energies and the three-body term ΔE_3:

$$\Delta E_{ABC} = \Delta E_{AB} + \Delta E_{AC} + \Delta E_{BC} + \Delta E_3 = E_{AB} - (E_A + E_B) + E_{AC} - (E_A + E_C) + E_{BC} - (E_B + E_C) + \Delta E_3 \quad (2)$$

Thus, the three-body term can be evaluated as

$$\Delta E_3 = E_{ABC} - E_{AB} - E_{AC} - E_{BC} + E_A + E_B + E_C \quad (3)$$

All interaction energies were calculated by using the optimized geometries of the complex and were corrected for the basis set superposition error in the trimer-centered basis set.[2] The deformation energies of the monomers were neglected because

TABLE 1: Selected Distances (Å) for Octahedral Complexes X−M_H−P (X = W or G) with the Outer-Shell Phosphate Coordination Optimized at the B3LYP/6-31+G(d) Level[a]

parameter\system	G−Mg−P	W−Mg−P	G−Cu−P	W−Cu−P	G−Zn−P	W−Zn−P	G−Cd−P	W−Cd−P
M−N7	2.243		2.099[b]		2.158		2.369	
M−W		2.129		2.382[b]		2.179		2.377
M−w1	2.098	2.089	2.302	1.977	2.139	2.104	2.345	2.331
M−w2	2.066	2.059	2.020	2.038	2.083	2.055	2.295	2.264
M−w3	2.097	2.081	2.011	2.230	2.119	2.085	2.310	2.294
M−w4	2.133	2.141	2.055	2.037	2.196	2.182	2.384	2.373
M−w5	2.138	2.133	2.399	2.087	2.197	2.188	2.402	2.385
w1−Op1	2.585	2.576	2.637	2.564	2.591	2.577	2.606	2.589
w2−Op2	2.567	2.538	2.615	2.528	2.547	2.520	2.556	2.531
w3−Op1	2.610	2.567	2.629	2.536	2.608	2.564	2.603	2.573
(O−H)w1	1.018	1.021	1.017	1.021	1.017	1.021	1.012	1.015
(O−H)w2	1.032	1.044	1.038	1.053	1.038	1.053	1.034	1.044
(O−H)w3	1.009	1.021	1.010	1.022	1.010	1.022	1.011	1.016
equil(O−H)	0.970							

[a] Constraints were utilized for Cu^{2+}, as specified above. [b] The Cu−L distances for octahedral (constrained) copper(II) complexes can be compared with those obtained for pentacoordinated ones (resulting from the full optimization of $[Cu^{II}(H_2O)_5(X)(H_2PO_4)]^+$ system) that can be found in Figure 2e,f.

TABLE 2: Selected Distances for Octahedral Complexes with the Inner-Shell Phosphate Coordination X−M_H−P_{in} (X = W or G) Obtained by the Optimization of Molecular Geometry at the B3LYP/6-31+G(d) Level[a]

parameter\system	G−Mg−P_{in}	W−Mg−P_{in}	G−Zn−P_{in}	W−Zn−P_{in}	G−Cd−P_{in}	W−Cd−P_{in}
M−N7	2.220		2.130		2.337	
M−W		2.119		2.176		2.393
M−Op	2.053	2.036	2.071	2.053	2.327	2.244
M−w1	3.612	3.341	3.590	3.554	3.699	3.697
M−w2	2.105	2.130	2.142	2.158	2.334	2.309
M−w3	2.151	2.098	2.206	2.157	2.402	2.378
M−w4	2.122	2.131	2.179	2.172	2.330	2.309
M−w5	2.120	2.135	2.173	2.093	2.373	2.383
w1−Op1	2.763	2.710	2.757	2.763	2.792	2.757
w2−Op2	2.672	2.641	2.670	2.710	2.664	2.591
w3−Op1	2.965	2.870	3.026	2.782	2.792	2.797
(O−H)w1	0.983	0.985	0.983	0.981	0.983	0.984
(O−H)w2	0.999	1.011	1.000	0.993	0.990	1.015
(O−H)w3	0.983	0.985	0.983	0.977	0.978	0.977
equil(O−H)	0.970					

[a] For the W−Zn_H−P_{in} complex, see also the text and Figure 2d.

they are an order of magnitude smaller than the interaction energies.[2] The deformation energy of a monomer is a repulsive contribution. It is caused by deformation of the monomer upon formation of the complex and is evaluated as the difference of total electronic energy of the monomer having the geometry in the complex and of the isolated relaxed monomer.

III. Results

IIIa. Analysis of Molecular Structures. The important geometrical parameters of the optimized molecular structures obtained with the DFT method are shown in Table 1 (X−M_H−P systems, X = G or W) and Table 2 (X−M_H−P_{in}). Several representatives of the optimized structures are depicted in Figure 2, including the pentacoordinate copper(II) complexes resulting from the full optimization of octahedral (Jahn−Teller unstable) initial structures. Namely, the tables contain metal−nucleobase distances (M−N7) and metal−water distances for the water molecule replacing the base (M−W). Furthermore, the metal−water oxygen distances for the remaining waters (M−w1 to M−w5) and oxygen−oxygen distances in the water bridges between M and P (w−Op) are explicitly listed together with the corresponding O−H bond lengths for the water bridges and the equilibrium O−H length for water molecules not involved in water bridges.

X−M_H−P Binding. The optimization of molecular geometries of G−M_H-P complexes resulted in the structures with inner-shell N7 binding of the metal ion and water molecules w1 and w3 interacting with one anionic oxygen; w1 is in cis position with respect to the nucleobase. Water w2 links the cation with the other anionic oxygen. Thus, the complex exhibits an outer-shell binding to the phosphate group via three water molecules. The remaining two water molecules form H-bonds to O6 of guanine. Replacing the guanine base by water W does not change the position of the remaining subsystems.

Comparison of Water−Cation and Nucleobase−Cation Interactions. The most salient observation that can be drawn from data in Table 1 is the variability of the N7−metal and metal−water distances for different metals. For Mg^{2+}, the N7−M distance is by 0.11−0.18 Å longer in comparison with M−w distances. Replacing Mg^{2+} with Zn^{2+} *shortens* the N7−M bond by 0.09 Å, whereas the M−w distances *increase* by 0.02−0.06 Å, especially for water molecules w4 and w5. Replacing guanine with the water molecule W considerably *shortens* the M−W distance compared to the M−N7 distance for the Mg^{2+} complex, whereas *elongation* occurs for the Zn^{2+} complex. It is noteworthy that the G → W substitution leads to minor contractions of the M−w distances for the other water molecules. Such contraction of the M−w distances indicates strengthening of the interaction. Again, the effect is considerably more pronounced for the Zn^{2+} complexes compared with their Mg^{2+} counterparts. *All the above distance redistributions upon Mg^{2+} → Zn^{2+} and G → W substitutions consistently show a substantial difference in the balance of water−metal and N7−metal interactions for Zn^{2+} and Mg^{2+}.* When Mg^{2+} is replaced with Zn^{2+}, the metal−N7 bond strengthens, whereas the metal−water interactions are weakened, making the water shell around Zn^{2+} substantially more flexible.[2,12f]

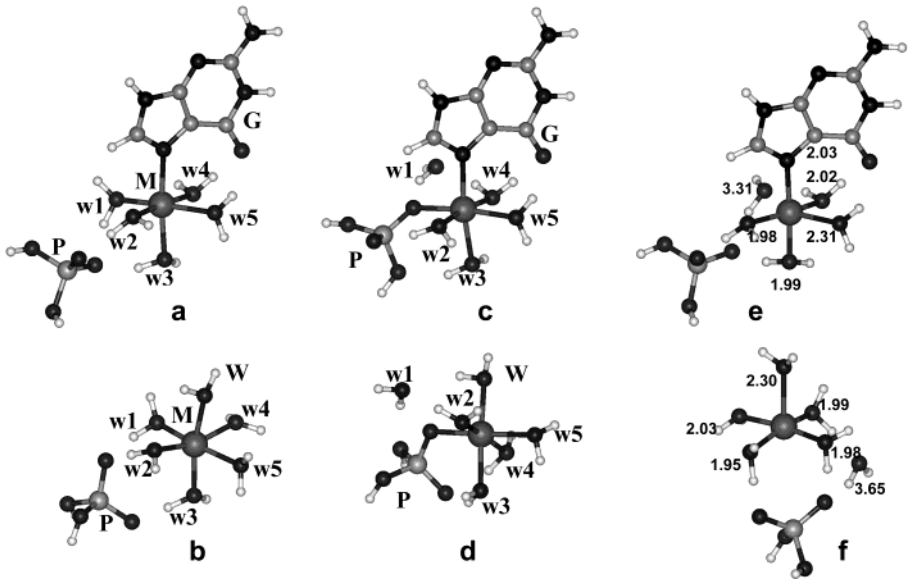

Figure 2. Optimized structures of several representatives of the studied complexes: (a) $[Zn(G)(H_2O)_5 \cdot (H_2PO_4)]^+$, (b) $[Zn(H_2O)_6 \cdot (H_2PO_4)]^+$, (c) $[Zn(G)(H_2O)_4(H_2PO_4) \cdot (H_2O)]^+$, (d) $[Zn(H_2O)_5(H_2PO_4) \cdot (H_2O)]^+$, (e) $[Cu(G)(H_2O)_4 \cdot (H_2PO_4)(H_2O)]^+$, (f) $[Cu(H_2O)_5 \bullet (H_2PO_4)\ (H_2O)]^+$. (a) and (b) represent outer-shell binding of phosphate, (c) and (d) are the inner-shell (denoted as P_{in}), and finally, (e) and (f) are the five-coordinate complexes of the copper(II) ion with the phosphate and water molecules in the second coordination shell (the M−L distances listed in 2e, 2f can be compared with the ones obtained for octahedrally constrained geometry; see Table 2).

Effect of Guanine Binding on Metal−Phosphate Recognition. The $Mg^{2+} \rightarrow Zn^{2+}$ substitution brings no changes in the Ow−Op distances and O−H covalent bond lengths in the metal−phosphate water bridges. Thus, the phosphate group does not discriminate whether it has outer-shell interaction with Zn^{2+} or Mg^{2+}, provided they have the same coordination mode. (Note that the possibility of substantial effects of the cation substitution on interactions between the first and second shell ligands has been discussed for different systems recently.[36]) On the other hand, all Ow−Op distances are contracted and O−H bonds extended (by 0.003−0.015 Å) when the G → W substitution is made. Thus, the phosphate group recognizes through its outer-shell binding when water is replaced by guanine on the opposite side of the cation coordination shell. The N7 binding *weakens* the outer-shell metal binding to the phosphate group, i.e., reduces polarization of the water molecules. Thus, a change of one ligand in the first coordination shell modifies the binding (on the opposite side of the shell) to the first coordination shell.

Cd^{2+} and Cu^{2+} Cations. In the Cd^{2+} complexes, all cation−ligand distances increase as Cd^{2+} has greater ionic radii than preceding two cations. However, the relative distribution of all the distances is essentially identical to Zn^{2+}. The evaluation of the Cu^{2+} complexes is less straightforward owing to the application of geometry constraints during the optimization (see the last paragraph of Introduction). Nevertheless, the distances indicate a strong relative preference for N7 binding, larger than for Zn^{2+}, which is in accord with IW series of stability constants and other studies.[16]

Water Bridges. The calculated structures show a large variability in the M−w distances, reflecting involvement of some of the water molecules in very strong water bridges. Shortening of the M−w distance in the M−w−A bridge is an indication of strengthening of the w−A H-bonding, thus, it is not surprising that the shortest M−w contact occurs in the M−w2−Op1 bridge, as there is only a single water bound to Op1. The formation of a metal−phosphate bridge is characterized by enormous elongations (0.04−0.08 Å) of the Ow−H bonds compared to the equilibrium value. This is considerably more than in conventional H-bonds and illustrates that there is a substantial polarization and charge transfer caused by the metal and mediated by the water molecules. The weaker water bridges toward O6 of guanine are characterized by O−H bond extension of ca. 0.1 Å (not shown).

$X-M_H-P_{in}$ Binding. In Table 2, DFT structural data for the $X-M_H-P_{in}$ (X = G or W) complexes with inner-shell binding of both X and P ligands are shown. The anionic Op1 oxygen forms an inner-shell contact with the metal ion. Water w1 is expelled into the second shell and is H-bonded to the same Op1 phosphate oxygen. This water bridge is rather weak due to a simultaneous metal binding to this oxygen and shift of w1 into the second shell. Water w2 forms a single water bridge to the Op2 phosphate oxygen, the strongest water bridge in the complex. Water w3 forms a weaker water bridge to one of the phosphate hydroxyl groups except of the $W-Zn_H-P_{in}$ DFT complex, where the phosphate group rotates and two water bridges to an anionic oxygen are formed (Figure 2d).

The $X-M_H-P_{in}$ complexes show the same *cation-dependent differences* of the balance in the N7−M and M−w distances as discussed above for the $X-M_H-P$ complexes. The inner-shell binding of the phosphate group leads to a shortening of the X−M distances (by 0.01−0.03 Å), indicating a subtle increase of the interaction upon the $X-M_H-P \rightarrow X-M_H-P_{in}$ transition. The metal−phosphate water bridges are evidently weaker than in the case of $X-M_H-P$ systems, which is demonstrated by the increase of the Op−w distances and shortening of the O−H bond. In fact, only the w2−Op2 water bridge remains strong. The role of water bridges in this system is clearly reduced due to the presence of the inner-shell contact of P to the metal. In contrast to the $X-M_H-P$ complexes, there is no indication of any systematic effect of the G → W substitution on the strength of the water bridges between the metal and the phosphate. On the other hand, there is a shortening of the Op1−M distance upon the G → W substitution. Thus, also in this binding mode, the phosphate group recognizes the G → W substitution and the nucleobase binding weakens the metal−phosphate contact. The shortening is ca. 0.02 Å for Mg^{2+} and Zn^{2+} but as much as 0.08 Å for Cd^{2+}. For Cd^{2+}, the G → W substitution also

TABLE 3: Energy Differences between $X-M_H-P_{in}$ and $X-M_H-P$ Complexes[a]

X	Mg^{2+}	Zn^{2+}	Cd^{2+}
G	−7.6 (−16.3)	−8.1 (−12.4)	−5.5 (−10.9)
W	−10.9 (−15.7)	−8.2 (−15.4)	−6.3 (−)

[a] The negative values indicate higher stability of the $X-M_H-P_{in}$ complex (calculated at the B3LYP level, values in parentheses are obtained at the MP2//HF level, in kcal·mol^{-1}).

strengthens the w2−Op2 bridge, as demonstrated by extension of the O−H bond by 0.025 Å. Note that the $W-Zn_H-P_{in}$ DFT complex shows a somewhat different interaction due to the phosphate rotation (see above).

Comparison of DFT and HF Data. In the Supporting Information (Table S1 and the pertinent paragraph), the structural data obtained at the HF/6-31G* level are summarized. The HF/6-31G* data allow comparison of the $G-M_H-P$ structures with those previously published for guanosine monophosphate (GMP^{-1}) interacting with pentahydrated cations through N7 inner-shell binding. This highlights the structural effects of the sugar deletion. In the M_H-GMP structures there are only two water bridges between the cation and the two anionic backbone oxygens. Thus, in nucleotides, the inner-shell M−N7 binding exerts some geometrical constraints on the metal−phosphate interaction. The metal−phosphate group water bridges in nucleotide have very similar geometries as the M−w3−Op single bridge here (cf. ref 2b, Table 2). Thus they are assumed to have a very similar strength. Interestingly, for all three metal cations, the M−N7 distance is consistently 0.05 Å smaller in the metalated nucleotides compared with the present study. This indicates a weaker N7−M interaction in the present system, which likely is due to formation of the third metal cation−phosphate group water bridge after sugar deletion and more efficient M_H-P interaction. Also, some charge transfer through the sugar unit could occur in the nucleotides. There is no effect on the specific differences between cations regarding the N7 binding selectivity. In summary, the sugar deletion seems to have only a modest effect on the molecular interactions in the studied system.

As a test, we reoptimized the G−Cd−P system at the HF level with the same basis set and pseudopotential as used in the DFT calculations (6-31+G(d,p) and SBJK). The optimized structure was almost identical to the HF/6-31G(d) one (not shown).

RI-MP2/TZVPP Geometries. As a test of the accuracy, we reoptimized the $X-Mg_H-P$ and $X-Mg_H-P_{in}$ complexes using resolution of the identity MP2 (RI-MP2) method with extended TZVPP basis set of atomic orbitals. When comparing our DFT and RI-MP2 geometries, we found a striking similarity confirming high accuracy of the DFT procedure. The M−N and M−O distances calculated with the reference RI-MP2/TZVPP method are systematically by ca. 0.02−0.03 Å shorter compared to the DFT data. The w−Op water bridge distances are contracted by ca. 0.04−0.06 Å. Accordingly, the O−H prolongation is marginally larger at the RI-MP2 level by about 0.005 Å. Thus, compared with the HF structures (see Supporting Information), the DFT geometries are substantially closer to the RI-MP2 ones. It confirms that the DFT geometries are superior to the HF ones.

IIIb. Analysis of Molecular Energies. In the following paragraphs we will complement the above structural analysis by a discussion of computed molecular energies of the studied molecular clusters.

Energy Difference between Inner- and Outer-Shell Binding of the Phosphate Moiety. In Table 3, the electronic energy differences between the $X-M_H-P$ and $X-M_H-P_{in}$ complexes are summarized. The inner-shell binding to phosphate (P_{in}) is favored over the outer-shell binding (P) in the gas phase. This is not surprising considering the direct interaction between the metal and the anionic oxygen in the $X-M_H-P_{in}$ binding mode. Note that the $X-M_H-P$ binding is more frequent in nucleic acids due to solvent screening and conformational restraints exerted by the backbone, nevertheless, examples of a simultaneous inner-shell binding of metals to nucleobases and backbone are also available, for example, in an RNA duplex with a bulged base and thus modified backbone topology.[4d] There is a rather significant difference between the DFT and MP2//HF data although both methods show the same trend (Table 3). The HF relative energies (not shown) are close to the MP2//HF ones. The leading energy term determining the difference between the two methods is the internal energy of the M_H subsystem. The reference RI-MP2/TZVPP difference between the $X-Mg_H-P_{in}$ and $X-Mg_H-P$ complexes is −11.2 and −8.2 kcal·mol^{-1} for X = W and G, respectively, differing by less than 1 kcal·mol^{-1} from the DFT values.

Energetics of (W → G) Substitution. In Table 4, the electronic energy changes caused by water to guanine (W → G) substitution calculated relative to W → G substitution in $X-Mg_H-P$ system are listed. The data confirm that Zn^{2+} and Cd^{2+} cations have higher affinity to the guanine base compared to Mg^{2+}, and this selectivity of binding is on a scale of ca. 3 kcal·mol^{-1}. The DFT and MP2//HF data are in a good agreement, except of the $X-Cd_H-P_{in}$ complex. There is ca. 3 kcal·mol^{-1} destabilization of the G(N7) binding of Mg^{2+} after the $P \rightarrow P_{in}$ change (the RI-MP2 method gives 3.0 kcal·mol^{-1} here).

Interaction Energies. In Tables 5 and 6, the DFT interaction energies for the $X-M_H-P$ and $X-M_H-P_{in}$ complexes are listed. The interaction energies are generally very sensitive gauges of a selectivity of the cation binding.

The complexes are divided into three subsystems: phosphate group (P), metal cation with water molecules w1−w5 (M_H), and the guanine base or water molecule W (X). The first column $X-M_H-P$ shows the total interaction energy of the trimer. The next three columns show the interaction energies calculated when the system is divided into two subsystems in three different ways. Thus, the M_H-XP term shows the interaction energy between the hydrated cation and the pocket formed by X and P, etc. The next three columns show the pairwise contributions and the last column is the three-body term. Obviously, the system could be further divided by considering the water molecules w1−w5 as separate subsystems. We have not carried out this rather complicated decomposition in the present study, but it has been done for smaller systems elsewhere.[2a]

Metal Ion Selectivity with Respect to N7 Binding. On the basis of the trimer interaction energy, the $W-Zn_H-P$ complex is by

TABLE 4: Energy Changes (kcal·mol^{-1}) Caused by the W → G(N7) Substitution, Calculated Relative to the Values for $X-Mg_H-P$ Complex

$X-Mg_H-P$	$X-Mg_H-P_{in}$	$X-Zn_H-P$	$X-Zn_H-P_{in}$	$X-Cd_H-P$	$X-Cd_H-P_{in}$
0.0 (0.0)	−3.3 (−4.1)	3.4 (3.2)	3.3 (1.5)	3.1 (−)	2.3 (−3.5)

[a] A negative value indicates that in the given complex the G → W substitution is favored relative to the $X-Mg_H-P$ complex. B3LYP data are reported, and the values in parentheses show the MP2//HF prediction.

TABLE 5: Interaction Energies (kcal·mol^{-1}) E_{12-3}, E_{1-23}, E_{13-2}, ... As Defined by Eqs 1−3 (X = H_2O or Guanine, M_H = $[M(H_2O)_5]^{2+}$, P = H_2PO_4)

X	method	ion	X−M_H−P	M_H−XP	XM_H−P	M_HP−X	X−M_H	X−P	M_H−P	ΔE_3
G	DFT	Mg^{2+}	−291.0	−296.3	−207.2	−59.3	−83.8	5.3	−231.6	19.1
	RI-MP2	Mg^{2+}	−295.7	−300.6	−212.0	−60.2	−83.7	4.9	−235.5	18.6
	DFT	Cu^{2+}	−316.2	−322.0	−215.4	−67.4	−100.8	5.8	−248.8	27.6
	DFT	Zn^{2+}	−296.5	−301.8	−208.7	−59.7	−87.7	5.4	−236.7	22.6
	DFT	Cd^{2+}	−288.0	−293.6	−204.8	−57.3	−83.1	5.7	−230.7	20.2
W	DFT	Mg^{2+}	−261.2	−263.3	−230.3	−23.1	−30.9	2.1	−238.1	5.6
	RI-MP2	Mg^{2+}	−265.7	−268.0	−233.5	−24.2	−32.2	2.3	−241.5	5.7
	DFT	Cu^{2+}	−273.0	−276.7	−246.6	−15.4	−26.4	3.7	−257.6	7.4
	DFT	Zn^{2+}	−262.6	−264.5	−234.7	−19.1	−27.9	1.9	−243.4	6.8
	DFT	Cd^{2+}	−255.1	−256.9	−228.9	−18.3	−26.2	1.8	−236.8	6.1

DFT/B3LYP (RI-MP2) calculations, X−M_H−P binding mode.

TABLE 6: Interaction Energies (kcal·mol^{-1}) E_{12-3}, E_{1-23}, E_{13-2}, ... As Defined by Eqs 1−3 (X = H_2O or Guanine, M_H = $[M(H_2O)_5]^{2+}$, P = H_2PO_4)

X	method	ion	X−M_H−P	M_H−XP	XM_H−P	M_HP−X	X−M_H	X−P	M_H−P	ΔE_3
G	DFT	Mg^{2+}	−318.0	−325.5	−226.9	−56.4	−91.1	7.5	−261.6	27.2
	RI-MP2	Mg^{2+}	−325.4	−331.7	−233.8	−59.7	−91.6	6.3	−265.7	25.6
	DFT	Zn^{2+}	−322.6	−330.5	−222.5	−58.7	−100.2	7.9	−263.9	33.6
	DFT	Cd^{2+}	−309.8	−313.1	−218.6	−58.7	−91.2	3.3	−251.1	29.1
W	DFT	Mg^{2+}	−286.1	−290.8	−253.1	−22.8	−33.0	4.7	−263.3	5.6
	RI-MP2	Mg^{2+}	−291.5	−297.0	−256.0	−24.4	−35.4	5.6	−267.0	5.4
	DFT	Zn^{2+}	−287.0	−290.5	−257.3	−19.3	−29.7	3.4	−267.7	6.9
	DFT	Cd^{2+}	−273.1	−277.3	−244.4	−17.5	−28.7	4.2	−255.6	7.0

DFT/B3LYP (RI-MP2) calculations, X−M_H−P_{in} binding mode.

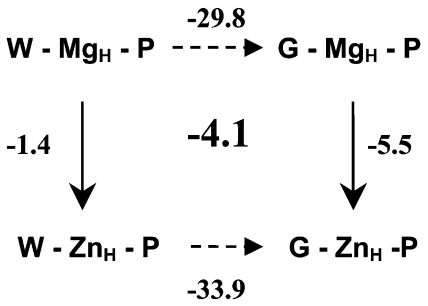

Figure 3. Changes of the trimer interaction energies upon various substitutions in the X−M_H−P system.

1.4 kcal·mol^{-1} more stable than its Mg^{2+} counterpart. This difference increases to 5.5 kcal·mol^{-1} when W is replaced by guanine G. Thus, the W → G substitution shifts the energy profile of the Mg^{2+} → Zn^{2+} exchange by −4.1 kcal·mol^{-1}. Note that the same number is obtained when calculating the Mg^{2+} → Zn^{2+} substitution effect on the energetics of the W → G substitution (Figure 3).

The above shift in interaction energy changes is the origin of the selectivity of the two cations with respect to N7. The shift originates in the X−M_H pairwise term where the change caused by the Mg^{2+} → Zn^{2+} substitution is −6.9 kcal·mol^{-1}. This difference, although reduced, carries to all terms where the X and M particles belong to different subsystems, i.e., M_H−XP (−4.2 kcal·mol^{-1}), M_HP−X (−4.4 kcal·mol^{-1}), and the whole complex X−M_H−P (−4.1 kcal·mol^{-1}). Note, that the phosphate group (cf. the M_H−XP, M_HP−X, and X−M_H-P values with the X−M_H term) reduces the difference due to screening of the interaction by the phosphate group. This can be well deduced from the 2.3 kcal·mol^{-1} change in the three-body term difference between W and G complexes ($\Delta\Delta E_3$) caused by the Mg^{2+} → Zn^{2+} substitution. The three-body term shows the polarization interligand repulsion between G and P subsystems as mediated by M_H.

The data for Mg^{2+} to Cd^{2+} substitution are similar though smaller in absolute value (approximately 3 kcal·mol^{-1}). A much larger preference for the W → G(N7) substitution compared to Mg^{2+} is indicated for Cu^{2+}, where the calculated shift for the X−M_H and X−M_H−P terms is −21.9 and −13.4 kcal·mol^{-1}, respectively. In addition to the clear preference of Cu^{2+} to bind to N7 compared to the other cations, Cu^{2+} is unable to maintain a stable hexa-coordination. The Cu^{2+} systems, being Jahn−Teller unstable in octahedral coordination geometry, spontaneously convert to the pentacoordinated geometry. The pentacoordinated geometry, on the other hand, is not a minimum for Mg^{2+}, preventing a direct comparison. This phenomenon (instability of certain coordination environment or a preference for the particular coordination geometry) makes the selectivity of metal ion−nucleobase interactions more variable.[13a]

Guanine Binding to the Metal Strongly Weakens the Metal−Phosphate Outer-Shell Interaction through Nonelectrostatic Effects. Table 5 also clearly shows that the W → G replacement reduces the strength of both XM_H−P and M_H−P terms. The former term is changed by ca. 20−30 kcal·mol^{-1}, the later by ca. 6−10 kcal·mol^{-1}. It is in excellent correlation with the above *geometrical* analysis predicting weakening of the through-water metal binding to phosphate upon the nucleobase binding to the metal. The XM_H−P term is expressed (see Computational Details) as the sum of M_H−P and X−P pairwise terms and the three-body term. In fact, the three-body term shows the largest change upon the W → G substitution (14−20 kcal·mol^{-1}), contrasting the small change in the X−P term. The leading role of the three-body term shows that this particular effect is of polarization/charge-transfer origin, with negligible pair electrostatic contribution. The aromatic nucleobase ligand affects the metal cation considerably more than the water molecule and reduces polarization of the remaining water molecules in the first hydration shell. It is then reflected in the values of O−H distances in the water bridges toward the phosphate group. The M_H−P pairwise term reflects these (secondary) geometry changes of the water bridges linking the two subsystems (see above) caused by the electronic structure redistribution primarily included in the three-body term. The effect of guanine binding on the strength of the metal−phosphate interaction is very

TABLE 7: Interaction Energies (kcal·mol^{-1}) As Defined by Eqs 1−3 and Calculated at the MP2/6-31G*//HF/6-31G* Level

X	ion	X−M_H-P	M_H−XP	XM_H−P	M_HP−X	X−M_H	X−P	M_H−P	ΔE_3
G	Mg^{2+}	−284.5	−290.7	−203.8	−58.8	−80.7	6.2	−225.7	15.7
	Zn^{2+}	−287.5	−293.7	−204.0	−59.6	−83.4	6.3	−227.8	17.5
	Cd^{2+}	−279.3	−285.7	−201.3	−56.0	−78.0	6.4	−223.2	15.5
W	Mg^{2+}	−255.8	−259.3	−222.5	−25.8	−33.6	3.5	−230.0	4.3
	Zn^{2+}	−254.4	−258.1	−223.9	−22.2	−30.5	3.4	−232.2	4.9
G, P_{in}	Mg^{2+}	−319.2	−327.1	−231.5	−55.9	−87.7	7.9	−263.3	23.9
	Zn^{2+}	−322.8	−331.7	−231.8	−57.4	−91.0	8.9	−265.4	24.7
	Cd^{2+}	−308.8	−317.9	−221.1	−54.7	−87.7	9.1	−254.1	23.9
W, P_{in}	Mg^{2+}	−290.6	−297.5	−253.3	−25.2	−37.3	6.9	−265.1	4.9
	Zn^{2+}	−286.2	−293.1	−251.8	−21.7	−34.4	6.9	−264.5	5.8
	Cd^{2+}	−276.5	−282.6	−242.7	−21.4	−33.8	6.1	−255.1	6.3

(X= H_2O or guanine, $M_H = [M(H_2O)_5]^{2+}$, P = H_2PO_4).

significant, in absolute values comparable to strength of guanine−cytosine base pair (ca. −26 kcal·mol^{-1})[37] and representing ca. 10% of the binding strength within the studied trimers. This kind of effect is neglected by conventional force fields whereas it substantially affects the balance of the actual binding of metal cations to nucleic acids.

Tables 5 and 6 also indicate that the $Cd^{2+} \rightarrow Mg^{2+}$ substitution leads to a selectivity change of 10 kcal·mol^{-1} (from 3 to 13 kcal·mol^{-1}) between G−M_H-P and W−M_H−P_{in} structures, relatively favoring the Cd^{2+} binding in the G−M_H−P mode (or destabilizing the W−Cd_H−P_{in}). Here the change of relative values of the X−M_H term is not dominating (3.5 kcal·mol^{-1}) and the leading term is the M_H-P contribution with a shift of 5.7 kcal·mol^{-1}. The $Cd^{2+} \rightarrow Mg^{2+}$ substitution substantially reduces the preference for the inner-shell binding of the metal to the anionic phosphate oxygen compared with the outer-shell binding, at least for the two water shell configurations compared. This could be a geometrical consequence of the larger radius of Cd^{2+} leading to a larger charge−charge separation in the interaction with negatively charged phosphate oxygens. The reduced preference of the W−Cd_H−P_{in} complex might seem to be in disagreement with the fact that the geometry optimization shows the outer-shell W−Cd_H−P complex unstable even as a local minimum for Cd^{2+} at the HF level. This, however, merely tells that there is no barrier for Cd^{2+} separating the W−M_H−P and W−M_H−P_{in} complexes at the HF level (in contrast to the other two cations), likely due to the larger radius of Cd^{2+} enabling an easier rearrangement of its coordination sphere. Note that DFT method shows two separate minima.

Comparison of DFT, MP2//HF, and RI-MP2 Data. In Tables 5 and 6, it is shown that for Mg^{2+}, the DFT and reference RI-MP2 approaches provide almost identical interaction energies. There is ca. 3−4 kcal·mol^{-1} difference in the M_H−P pairwise term that obviously also affects XM_H−P, M_H−PX, and X−M_H−P data. The remaining contributions are essentially identical.

The MP2//HF data (Table 7) compare rather well with the DFT calculations with the largest differences in individual terms being smaller than 10 kcal·mol^{-1}. Both methods predict identical relative trends regarding the selectivity of cation binding and the destabilizing effect of the guanine binding on the metal−phosphate interaction. The latter effect is underestimated by a few kcal·mol^{-1} for reasons explained in the section regarding the geometries.

The MP2//HF data can be directly compared with previously studied dGMP^{-1}−M_H complexes analyzed at the same level.[2b] (dGMP^{-1} stands for deoxyribonucleotide monophosphate). The dGMP^{-1}−M_H term is −270.8 for Mg^{2+} and −275.1 kcal·mol^{-1} for Zn^{2+},[2b] thus being 20 kcal·mol^{-1} lower in absolute values than the present M_H-GP terms. This reflects a better optimization of the interaction in absence of the constraints exerted by the sugar unit, though the relative difference is not large.

TABLE 8: Solvation Gibbs Energies (kcal·mol^{-1}) Calculated in the Framework of CPCM (COSMO) Model at the B3LYP/6-31G(d) Level for $[MX(H_2O)_5]^{2+}\cdot(H_2PO_4^-)$ and $[MX(H_2O)_4(H_2PO_4)]^{+}\cdot(H_2O)$ Complexes

X	binding mode	Mg^{2+}	Cu^{2+}	Zn^{2+}	Cd^{2+}
G	P	−66.1	−66.4	−65.7	−62.9
	P_{in} (P_5 for Cu^{2+})	−57.8	−62.2	−57.5	−56.4
W	P	−69.3	−68.6	−68.5	−64.4
	P_{in} (P_5 for Cu^{2+})	−60.0	−62.7	−60.6	−59.4

Interaction vs Total Energies. The trimer interaction energies (Tables 5 and 6) indicate a much larger preference of the X−M_H−P_{in} complexes with respect to the X−M_H−P ones (ca. 20−30 kcal·mol^{-1}) compared to the data based on absolute (total, electronic) energies (around 5−10 kcal·mol^{-1}, Table 3). This can be explained in the following way. The W−M_H−P → W−M_H−P_{in} transition is associated with a substantial improvement of the M_H−P interaction; however, the internal energy of the M_H subsystem deteriorates by ca. 20−25 kcal·mol^{-1} due to an expulsion of one water molecule into the second shell. The second contribution is neglected when the interaction energies are evaluated and the hydrated metal is one subsystem whereas it is fully included in the total electronic energies. Thus, to obtain completely insight into the balance of interactions in the studied complexes, one preferably should take into account both interaction energies of subsystems and total electronic energies.

IIIc. Entropy and Solvation Effects. All the above calculations were carried out by assuming a medium-sized molecular cluster in the gas phase, where the solvent effects were included only via the first hydration shell. Because the kinetics and thermodynamics of the processes occurring in the (bio)chemical systems in solution is determined by the Gibbs energy content of participating species, we estimated additional continuum solvation effects accompanying the outer-shell and inner-shell binding of phosphate group to the hydrated metal ions. The calculated Gibbs solvation energies are listed in Table 8. It can be seen that though, as can be expected for ionic species, their values are large (−56 to −69 kcal·mol^{-1}), they are *almost constant* for a particular X group (G or W) and binding mode. We feel obliged to present these results as to demonstrate the transferability of the preceding gas-phase results and subsequent discussions to the solution phase. However, it must be stressed that it is possible only for the relative trends obtained for the series of TM ions with *the same charge*. Thus, the presented gas-phase values with inclusion of the first hydration shell should yield an accurate enough basis for the discussion regarding the *nonelectrostatic specificity* of the binding of metal ions with the same charge to RNA/DNA molecules and their relative values would not be influenced by the solvation effects to a great extent. As pointed out elsewhere, in metal cation

containing systems the solvent screening effects tend to annihilate the ionic pair electrostatic contributions whereas the major part of nonelectrostatic contributions is conserved.[22]

IV. Discussion and Conclusions

We have carried out a series of quantum chemical investigations of structures and energies of complexes between several hydrated divalent cations and nucleic acid constituents. Our calculations include inner-shell cation binding to N7 of guanine and inner- and outer-shell cation binding to the phosphate group. The calculations mimic the binding of the cations to nucleotide or ribonucleotide. However, by deleting the sugar unit, we are able to separate the metal−nucleobase and metal−phosphate contacts and can study their mutual electronic structure influence.

An explicit comparison of structures and energies of the outer-shell complexes with and without[2b] the sugar deletion reveals only a modest effect of the deletion on the metal−phosphate and metal−nucleobase binding that can be rationalized as a result of optimization of the hydrated metal−phosphate interaction in absence of the constraints imposed by the sugar moiety. It indicates that our reduced model complex is entirely realistic. In general, sugar moieties are not preferable metal-binding sites in nucleic acids and mostly show no marked interactions even with the first ligand shell of the metal cation. Thus sugar does not have any major influence on the nature of metal−nucleotide interaction (as indicated also by the limited comparison with full metal−GMP^{-1} calculations commented on above). The sugar nevertheless can impose certain geometrical restraints that could affect the binding preferences. However, these conformational restraints imposed by the sugar unit are likely variable in different systems, ranging from nucleotides, through single strands, duplexes (A, B, and Z forms), other shapes such as loops, bulges, the different multiple-stranded architectures, complex non-W.C. RNA motifs, various tertiary complexes, etc. Nucleic acids form an astonishing variety of architectures, and to analyze the effect of sugar on metal binding, each structural type should be investigated separately. We are presently working on a more thorough analysis of the effect of the sugar conformation on several inner- and outer-shell metal-binding motifs to GMP^{-1}, and the results will be published in a forthcoming paper.

In the present study, we analyze geometries and energies of the complexes. The molecular geometry represents indispensable information to highlight the nature and strength of molecular interactions in larger cationic clusters. It is because the information obtained by interaction energy analysis is limited due to large nonadditivities of molecular interactions. Thus pairwise interaction energy terms may be misleading for evaluation of the interaction between two selected groups. On the other hand, detailed geometrical features, such as distribution of metal−ligand distances and O−H bond stretching in water bridges nicely reflect the balance of interactions determining the selectivity of binding. When comparing the structural and energetical data, we conclude that both approaches complement each other and for most cases exhibit identical trends. On the basis of our preceding experience, we did not attempt charge distribution analyses, as atomic charges are not uniquely defined and they are method-dependent. We would like to strongly argue against any utilization of Mulliken population analysis. Calculated Mulliken charges on metal cations can, in systems such as those studied here, drastically vary (by 0.3−0.4 e) with marginal changes of the basis set of atomic orbitals. Nevertheless, several sophisticated atomic charge distribution schemes are presently available and could be used as an additional analytical tool.

We have applied three computational approaches. Becke3LYP/6-311++G(2df,2pd)//Becke3LYP/6-31+G(d), MP2/6-31G(d)//HF/6-31G(d), and RI-MP2/TZVPP//RI-MP2//TZVPP methods. (The abbreviation A//B denotes that molecular geometries are obtained by method B and the final single-point molecular energies by method A.) The DFT/Becke3LYP approach is considered more accurate for the present systems compared to the MP2/6-31G(d)//HF/6-31G(d) method that has been widely used in the past. Nevertheless, it is encouraging to see that all major trends studied in this paper are predicted by both methods, although they are more apparent at the DFT level. Pilot calculations carried out using the RI-MP2/TZVPP//RI-MP2//TZVPP method for Mg^{2+} containing complexes show that the DFT geometries and energies are in excellent agreement with the RI-MP2 data whereas the HF geometries are less accurate. The RI-MP2 method could represent a method of choice in related studies soon, as it is considerably faster compared to conventional MP2 with close to identical results.[34] Thus it allows to routinely use extended basis set like the TZVPP one (equivalent in quality to cc-pVTZ basis set) used here. It nevertheless appears that the DFT method with large basis set of atomic orbitals provides almost identical results for the present ionic systems and has been extensively verified recently also for open shell systems.[13,14,17]

The calculations illustrate that the cations have different balance of water−cation and N7−cation binding, leading to selectivity toward the N7 binding in the following order: $Cu^{2+} \gg Zn^{2+} = Cd^{2+} > Mg^{2+}$. It is consistently reflected by changes of interatomic distances upon cation substitution, changes of absolute electronic energies and by interaction energies. Further, the Cu^{2+} cation is unable to attain a stable hexacoordinated geometry, contrasting the other three cations and contributing to the diversity of binding. The energetics of the cation selectivity is typically on a scale of 3−10 kcal·mol^{-1}. It may seem to be a negligible contribution, comparing with the overall binding energies around −300 kcal·mol^{-1}. Note, however, that the large absolute values of interaction energies are due to the ionic nature of the interaction. When transferring the complexes into a polar solvent, these large electrostatic terms are essentially annihilated whereas the nonelectrostatic (polarization and charge transfer) contributions are much less affected. Then the nonelectrostatic effects of just a few kcal·mol^{-1} become of utmost importance. The small energy scale of the cation selectivity is actually needed to provide enough flexibility for the cation binding and the actual binding is also strongly influenced by the DNA/RNA shapes and compositions. Then the cations can play multiple roles and often, though not always, substitute one for another. For example, although a simultaneous inner-shell binding of Mg^{2+} to nucleobase N7 and phosphate is predicted by the calculations as a relatively poor binding option compared with the other metals, it has already been detected in an RNA duplex with a single base bulge.[4d] The tiny energy scale of selectivity is typical for molecular recognition in biopolymers. The selectivity scale of a few kcal·mol^{-1} is consistent with recently calculated data for a number of metal cations toward different protein binding sites.[17] It must be noted that a meaningful calculation of selectivity of cation binding requires the inclusion of the complete first coordination sphere of the cation into calculations. For bare ions, the Zn^{2+} vs Mg^{2+} selectivity regarding the water → guanine substitution rises to ca. 25 kcal·mol^{-1} (an order of magnitude) which bears no relevance for biological systems.[2a]

Our calculations show that the inner-shell binding to the phosphate (P_{in}) is more stable than the outer-shell binding (P) in the presently studied model molecular cluster. It however does not mean that this conclusion can be generalized. There are always complex interplays between the intrinsic interaction terms as studied by our calculations and all the solvent effects, salt, conformational type and composition of nucleic acid structures, crystal lattice effects in X-ray experiments (majority of divalent metals seen in X-ray experiments are involved in crystal lattice contacts), etc. All these factors affect the P vs P_{in} balance in nucleic acids; thus, a general prediction regarding which of them is more stable in nucleic acids is not possible. Both P_{in} and P motifs are entirely relevant and occur in nucleic acids. Each particular type of nucleic acid (NA molecule) would have to be studied separately to ultimately evaluate its unique metal binding preferences. The main effort of our paper was to describe the physicochemical origin of the metal binding and qualitative interaction trends within different binding modes. This obviously represents one of the major pieces of information needed to evaluate stability of different binding modes in nucleic acids.

The calculations revealed yet another major nonelectrostatic contribution. Inner-shell binding of guanine to the metal cation (water to guanine substitution in the first shell around the metal cation) substantially reduces the strength of the outer-shell binding of the metal to the phosphate group. The effect is on an energy scale of ca. 25 kcal·mol^{-1} that is very strong and is evidenced by a considerable reduction of the O−H bond stretching in the metal−phosphate water bridges upon guanine binding. The primary reason is a reduction of hydrogen bonding capability of the polarized first-shell water molecules due to polarization and charge transfer toward the aromatic nucleobase. Thus, the phosphate directly recognizes whether the cation is bound to the nucleobase or not. Effects of this kind, neglected by conventional force fields, inevitably contribute to distribution of divalent cations around nucleic acids. To a considerably lesser amount, the type of cation affects the strength of its outer-shell binding to the phosphate group. In this particular case the role of the cation size is evident though some nonelectrostatic effects are likely present.

In the present study, we focused our attention on major nonelectrostatic interactions (see the introduction for the definition) that are completely neglected in contemporary nucleic acids molecular dynamics simulations, electrostatic Poisson−Boltzmann calculations or Brownian Dynamics with charged probes and other methods not based on molecular orbital theory.[38] We do not argue against utilization of simple empirical potential methods. Such calculations allow obtaining very valuable insights into systems considerably larger compared to those treatable by molecular orbital calculations. However, the results of empirical potential studies should, to our opinion, be presented more carefully compared to the current practice and in the context of the quantum-chemical studies. The present lack of relevant discussions of force-field approximations may lead to unnecessary disappointments regarding the performance of MD and Brownian dynamics simulations for cations soon.[39] Note, for example, that despite the overall good performance of MD simulations for *monovalent* cation-stabilized guanine quadruplex molecules, several apparent disagreements with high-resolution crystals have been recently identified, and attributed to the lack of polarization and charge transfer in the force field.[38c,39] Inevitably, limitations in description of *divalent* cations are much larger. The nonelectrostatic contributions represent one of the major factors determining the selectivity of metal binding to nucleic acids.

Acknowledgment. This work was supported by projects LN00A032 (J.S., Center for Complex Molecular Systems and Biomolecules), Z4055905 (L.R.) and grant A4055103/01 (L.R., GA AV CR). CPU time on Origin 2000 at MU Brno (project MetaCentre) and NEC-SX4 at CHMI (Grant No. LB98202, project INFRA2 of MSMT CR) is gratefully acknowledged.

Supporting Information Available: The geometries and molecular energies of all the studied systems, comparative geometry of one cation−nucleotide system and selected distances in HF-optimized complexes are available free of charge via the Internet at http://pubs.acs.org.

References and Notes

(1) (a) Ghosh, P.; Shabat, D.; Kumar, S.; Sinha, S. C.; Grynszpan, F.; Li, J.; Noodleman, L.; Keinan, E. *Nature* **1996**, *382*, 339. (b) Pierloot, K.; De Kerpel, J. O. A.; Ryde, U.; Olsson, M. H. M.; Roos B. O. *J. Am. Chem. Soc.* **1998**, *120*, 13156. (c) De Kerpel, J. O. A.; Pierloot, K.; Ryde, U. *J. Phys. Chem. B* **1999**, *103*, 8375. (d) Noy, D.; Yerushalmi, R.; Brumfeld, V.; Ashur, I.; Scheer, H.; Baldridge, K. K.; Scherz, A. *J. Am. Chem. Soc.* **2000**, *122*, 3937. (e) Lovell, T.; Li, J.; Liu, T.; Case D. A.; Noodleman, L. *J. Am. Chem. Soc.* **2001**, *123*, 12392. (f) Davis, M. I.; Orville, A. M.; Neese, F.; Zaleski, J. M.; Lipscomb, J. D.; Solomon, E. I. *J. Am. Chem. Soc.* **2002**, *124*, 602.

(2) (a) Šponer, J.; Burda, J. V.; Sabat, M.; Leszczynski, J.; Hobza, P. *J. Phys. Chem. A* **1998** *102*, 5951. (b) Šponer, J.; Sabat, M.; Gorb, L; Leszczynski, J.; Lippert, B.; Hobza, P. *J. Phys. Chem. B* **2000**, *104*, 7535.

(3) (a) Ryde, U.; Olsson, M. H. M. *Int. J. Quantum Chem.* **2001**, *81*, 335. (b) Olsson, M. H. M.; Ryde, U. *J. Am. Chem. Soc.* **2001**, *123*, 7866.

(4) (a) Correll, C. C.; Freeborn, B.; Moore, P. B.; Steitz, T. A. *Cell* **1997**, *91*, 705. (b) Harper, A.; Brannigan, J. A.; Buck, M.; Hewitt, L.; Lewis, R. J.; Moore, M. H.; Schneider, B. *Acta Crystallogr. D, Biol. Crystallogr.* **1998**, *54*, 1273. (c) Soler-Lopez, M.; Malinina, L.; Liu, J.; Huynh-Dinh, T.; Subirana, J. A. *J. Biol. Chem.* **1999**, *274*, 23683. (d) Ennifar, E.; Yusupov, M.; Walter, P.; Marquet, R.; Ehresmann, B.; Ehresmann, C.; Dumas, P. *Struct. Fold. Des.* **1999**, *7*, 1439. (e) Abrescia, N. G. A.; Malinina, L.; Fernandez, L. G.; Huynh-Dinh, T.; Neidle, S.; Subirana, J. A. *Nucl. Acids Res.* **1999**, *27*, 1593. (f) Cate, J. H.; Hanna, R. L.; Doudna, J. A. *Nat. Struct. Biol.* **1997**, *4*, 553. (g) McKay, D. B. *RNA* **1996**, *2*, 395. (h) Tereshko, V.; Wilds, C. J.; Minasov, G.; Prakash, T. P.; Maier, M. A.; Howard, A. Wawrzak, Z. Manoharan, M.; Egli, M. *Nucl. Acids Res* **2001**, *29*, 1208. (i) Shui, X. Q.; Sines, C. C.; McFail-Isom, L.; VanDerveer, D.; Williams, L. D. *Biochemistry* **1998**, *37*, 16877. (j) For a recent crystallographic review on DNA−metal binding see: Egli, M. *Chem. Biol.* **2002**, *9*, 277.

(5) (a) Lippert, B. *Coord. Chem. Rev.* **2000**, *200*, 487. (b) Sigel, R. K. O.; Freisinger, E.; Lippert, B. *J. Biol. Inorg. Chem.* **2000**, *5*, 287.

(6) Marzilli, L. G.; Ano, S.; Intini, F. P.; Natile, G. *J. Am. Chem. Soc.* **1999**, *121*, 9133.

(7) (a) Siegbahn, P. E. M.; Crabtree, R. H. *J. Am. Chem. Soc.* **1999**, *121*, 117. (b) Siegbahn, P. E. M. *Inorg. Chem.* **2000**, *39*, 2923. (c) Li, J.; Nelson, M. R.; Peng, C. Y.; Bashford, D.; Noodleman, L. *J. Phys. Chem. A* **1998**, *102*, 6311. (d) Li, J.; Fisher, C. L.; Konecny, R.; Bashford, D.; Noodleman, L. *Inorg. Chem.* **1999**, *38*, 929. (e) Konecny, R.; Li, J.; Fisher, C. L.; Dillet, V.; Bashford, D.; Noodleman, L. *Inorg. Chem.* **1999**, *38*, 940. (f) Himo, F.; Eriksson, L. A.; Maseras, F.; Siegbahn, P. E. M. *J. Am. Chem. Soc.* **2000**, *122*, 8031. (g) Siegbahn, P. E. M. *J. Biol. Inorg. Chem.* **2001**, *6*, 27.

(8) (a) Niu, S.; Hall, M. B. *Chem. Rev.* **2000**, *100*, 353. (b) Loew, G. H.; Harris, D. L. *Chem. Rev.* **2000**, *100*, 407. (c) Siegbahn, P. E. M.; Blomberg, M. R. A. *Chem. Rev.* **2000**, *100*, 421. (d) Frenking, G.; Fröhlich, N. *Chem. Rev.* **2000**, *100*, 717. (e) Hush, N. S.; Reimers, J. R. *Chem. Rev.* **2000**, *100*, 775.

(9) Siegbahn, P. E. M.; Blomberg, M. R. A. *Annu. Rev. Phys. Chem.* **1999**, *50*, 221.

(10) Bluhm, B. K.; Shields, S. J., Bayse C. A.; Hall, M. B.; Russell, D. H. *Int. J. Mass. Spectrom.* **2001**, *204*, 31.

(11) Vrettos, J. S.; Stone, D. A.; Brudvig, G. W. *Biochemistry* **2001**, *40*, 7937.

(12) (a) Garmer, D. R.; Gresh, N. *J. Am. Chem. Soc.* **1994**, *116*, 3556. (b) Gresh, N.; Garmer, D. R. *J. Comput. Chem.* **1996**, *17*, 1481. (c) Garmer, D. R.; Gresh, N.; Roques, B. P. *Proteins Struct. Funct. Genet.* **1998**, *31*, 42. (d) Dudev, T.; Cowan, J. A.; Lim, C. *J. Am. Chem. Soc.* **1999**, *121*, 7665. (e) Dudev, T.; Lim, C. *J. Am. Chem. Soc.* **2000**, *122*, 11146. (f) Dudev, T.; Lim, C. *J. Phys. Chem. B* **2001**, *105*, 4446. (g) Bock, C. W.; Katz, A.

K.; Markham, G. D.; Glusker, J. P. *J. Am. Chem. Soc.* **1999**, *121*, 7360. (h) Bock, C. W.; Katz, A. K.; Glusker, J. P. *J. Am. Chem. Soc.* **1995**, *117*, 3754. (i) Rodriguez-Santiago, L.; Sodupe, M.; Tortajada, J. *J. Phys. Chem. A* **2001**, *105*, 5340. (j) Bertran, J.; Rodriguez-Santiago, L.; Sodupe M. *J. Phys. Chem. B* **1999**, *103*, 2310.

(13) (a) Rulíšek, L.; Vondrášek J. *J. Inorg. Biochem.* **1998**, *71*, 115. (b) Rulíšek, L.; Havlas, Z. *J. Am. Chem. Soc.* **2000**, *122*, 10428.

(14) Rulíšek, L.; Havlas, Z. *J. Phys. Chem. A* **2002**, *106*, 3855.

(15) (a) Pearson, R. G. *J. Am. Chem. Soc.* **1963**, *85*, 3533. (b) Parr, R. G.; Pearson, R. G. *J. Am. Chem. Soc.* **1983**, *105*, 7512.

(16) (a) Irving, H.; Williams, R. J. P. *Nature* **1948**, *162*, 746. (b) Sigel, H.; McCormick, D. B. *Acc. Chem. Res.* **1970**, *3*, 201.

(17) (a) Rulíšek, L.; Havlas, Z. *J. Phys. Chem. A* **1999**, *103*, 1634. (b) Rulíšek, L.; Havlas, Z. *J. Chem. Phys.* **2000**, *112*, 149.

(18) (a) Šponer, J.; Burda J. V.; Mejzlík, P.; Leszczynski, J.; Hobza, P. *J. Biomol. Struct. Dyn.* **1997**, *14*, 613. (b) Famulari, A.; Moroni, F.; Sironi, M.; Raimondi, M. *Comput. Chem.* **2000**, *24*, 341. (c) Pelmenschikov, A.; Zilberberg, I.; Leszczynski, J.; Famulari, A.; Sironi, M.; Raimondi, M. *Chem. Phys. Lett.* **1999**, *314*, 496. (d) Burda, J. V.; Šponer, J.; Leszczynski, J. *Phys. Chem. Chem. Phys.* **2001**, *3*, 4404. (e) Muñoz, J.; Gelpí, J. L.; Soler-Lopez, M.; Subirana, J. A.; Orozco, M.; Luque, F. J. *J. Phys. Chem B* **2002**, *106*, 0000.

(19) (a) Šponer, J.; Sponer, J. E.; Leszczynski, J. *J. Biomol. Struct. Dyn.* **2000,** *17*, 1087. (b) Petrov, A. S.; Lamm, G.; Pack, G. R. *J. Phys. Chem. B* **2002**, *106*, 3294.

(20) Šponer, J. E.; Glahe, F.; Leszczynski, J.; Lippert, B.; Šponer, J. *J. Phys. Chem. B* **2001**, *105*, 12171.

(21) Gresh, N.; Šponer, J. *J. Phys. Chem. B* **1999**, *103*, 11415.

(22) (a) Burda, J. V.; Šponer, J.; Leszczynski, J. *J. Biol. Inorg. Chem.* **2000**, *5*, 178. (b) Šponer, J.; Šponer, J. E.; Gorb, L.; Leszczynski, J.; Lippert, B. *J. Phys. Chem. A* **1999**, *103*, 11406. (c) Šponer, J. E.; Leszczynski, J.; Glahe, F.; Lippert, B.; Šponer, J. *Inorg. Chem.* **2001**, *40*, 3269.

(23) (a) Gu, J. D.; Leszczynski, J. *J. Phys. Chem A* **2002**, *106*, 529. (b) Meyer, M.; Steinke, T.; Brandl, M.; Suhnel, J. *J. Comput. Chem.* **2001**, *22*, 109.

(24) (a) Deubel, D. V. *J. Am. Chem. Soc.* **2002**, *124*, 5834. (b) Baik, M. H.; Friesner, R. A.; Lippard, S. J. *J. Am. Chem. Soc.* **2002**, *124*, 4495.

(25) (a) Schneider, B.; Kabelac, M.; Hobza, P. *J. Am. Chem. Soc.* **1996**, *118*, 8, 12207. (b) Yang, E.; Zhou, L. X.; Zhang, Y. F. *Chin. J. Struct. Chem.* **2002**, *21*, 103. (c) Murashov, V. V.; Leszczynski, J. *J. Phys. Chem. B* **1999**, *103*, 8391.

(26) Frisch, M. J.; Trucks, G. W.; Schlegel, H. B.; Scuseria, G. E.; Robb, M. A.; Cheeseman, J. R.; Zakrzewski, V. G.; Montgomery, J. A., Jr.; Stratmann, R. E.; Burant, J. C.; Dapprich, S.; Millam, J. M.; Daniels, A. D.; Kudin, K. N.; Strain, M. C.; Farkas, O.; Tomasi, J.; Barone, V.; Cossi, M.; Cammi, R.; Mennucci, B.; Pomelli, C.; Adamo, C.; Clifford, S.; Ochterski, J.; Petersson, G. A.; Ayala, P. Y.; Cui, Q.; Morokuma, K.; Malick, D. K.; Rabuck, A. D.; Raghavachari, K.; Foresman, J. B.; Cioslowski, J.; Ortiz, J. V.; Stefanov, B. B.; Liu, G.; Liashenko, A.; Piskorz, P.; Komaromi, I.; Gomperts, R.; Martin, R. L.; Fox, D. J.; Keith, T.; Al-Laham, M. A.; Peng, C. Y.; Nanayakkara, A.; Gonzalez, C.; Challacombe, M.; Gill, P. M. W.; Johnson, B.; Chen, W.; Wong, M. W.; Andres, J. L.; Gonzalez, C.; Head-Gordon, M.; Replogle, E. S.; Pople, J. A. *Gaussian 98*, Revision A.6; Gaussian, Inc.: Pittsburgh, PA, 1998.

(27) Becke, A. D. *J. Chem. Phys.* **1993**, *98*, 5648.

(28) (a) Becke, A. D. *Phys. Rev. A* **1988**, *38*, 3098. (b) Lee, C.; Yang, W.; Parr, R. G. *Phys. Rev. B* **1988**, *37*, 785. (c) Vosko, S. H.; Wilk, L.; Nusair, M. *Can. J. Phys.* **1980**, *58*, 1200.

(29) (a) Watchers, A. J. H. *J. Chem. Phys.* **1970**, *52*, 1033. (b) Hay, P. J. *J. Chem. Phys.* **1977**, *66*, 4377. (c) Raghavachari, K.; Trucks, G. W. *J. Chem. Phys.* **1989**, *91*, 1062.

(30) (a) McLean, A. D.; Chandler, G. S. *J. Chem. Phys.* **1980**, *72*, 5639. (b) Krishnan, R.; Binkley, J. S.; Seeger, R.; Pople, J. A. *J. Chem. Phys.* **1980**, *72*, 650.

(31) Stevens, W. J.; Krauss, M.; Basch, H.; Jasien, P. G. *Can. J. Chem.* **1992**, *70*, 612.

(32) Hurley, M. M.; Pacios, L. F.; Christiansen, P. A.; Ross, R. B.; Emler, W. C. *J. Chem. Phys.* **1986**, *84*, 6840.

(33) (a) Ahlrichs, R.; Bar, M.; Haser, M.; Horn, H.; Kolmel, C. *Chem. Phys. Lett.* **1989**, *162*, 165. (b) Feyresein, M.; Fitzgerald, G.; Komornicky, A. *Chem. Phys. Lett.* **1993**, *208*, 359. (c) Weigend, F.; Haser, M.; Patzelt, H.; Ahlrichs, R. *Chem. Phys. Lett.* **1998**, *294*, 143.

(34) (a) Jurecka, P.; Nachtigall, P.; Hobza, P. *Phys. Chem. Chem. Phys.* **2001**, *3*, 4578. (b) Hobza, P.; Sponer, J. *J. Am. Chem. Soc.* **2002**, *124*, 11802.

(35) (a) Klamt, A.; Schuurmann, G. *J. Chem. Soc. Perkin Trans. 2* **1993**, 799. (b) Barone, V.; Cossi, M.; Tomasi, J. *J. Comput. Chem.* **1998**, *19*, 404.

(36) (a) Walker, N.; Dobson, M. P.; Wright, R. R.; Barran, P. E.; Murrell, J. N. Stace A. J. *J. Am. Chem. Soc.* **2000**, *122*, 11138. (b) Stace, A. J.; Walker, N. R.; Firth, S. *J. Am. Chem. Soc.* **1997**, *119*, 10239. (c) Berces, A.; Nukada, T; Margl, P.; Ziegler, T. *J. Phys. Chem. A* **1999**, *103*, 9693.

(37) (a) Šponer, J.; Leszczynski, J.; Hobza, P. *Biopolymers* **2001**, *61*, 3. (b) Šponer, J.; Hobza, P. *J. Phys. Chem. A* **2000**, *104*, 4592.

(38) (a) Young, M. A.; Ravishanker, G.; Beveridge, D. L. *Biophys. J.* **1997**, *73*, 2313. (b) Špačková, N.; Berger, I.; Šponer, J. *J. Am.Chem. Soc.* **2001**, *123*, 3295. (c) Špačková, N.; Berger, I.; Šponer, J. *J. Am. Chem. Soc.* **1999**, *121*, 5519. (d) Csaszar, K.; Špačková, N.; Štefl, R.; Šponer, J.; Leontis, N. B. *J. Mol. Biol.* **2001**, *313*,1073. (e) Burkhardt, C.; Zacharias, M. *Nucl. Acids Res.* **2001**, *29*, 3910. (f) Hermann, T.; Auffinger, P.; Scott, W. G.; Westhof, E. *Nucl. Acids Res.* **1997**, *25*, 3421. (g) Martinez, J. M.; Elmroth, S. K. C.; Kloo, L. *J. Am. Chem. Soc.* **2001**, *123*, 12279. (h) Misra, V. K.; Draper, D. E. *Proc. Natl. Acad. Sci. U.S.A.* **2001**, *98*, 12456. (i) van Buuren, B. N. M.; Hermann, T**.** Wijmenga, S. S.; Westhof, E. *Nucl. Acids Res.* **2002**, *30*, 507. (j) Hermann, T.; Westhof, E. *Structure* **1998**, *6*, 1303.

(39) Haider, S.; Parkinson, G. N.; Neidle, S. *J. Mol. Biol.* **2002**, *320*, 189−200.